

A High-accuracy SINS/CNS Integrated Navigation Scheme Based on Overall Optimal Correction

Jiafang Zhu¹, Xinlong Wang¹, Hengnian Li², Huan Che³ and Qunsheng Li⁴

¹(School of Astronautics, Beihang University, China)

²(State Key Lab of Astronautical Dynamics, Xi'an Satellite Control Center, Xi'an 710043, China)

³(Space Star Technology Co., Ltd, Beijing 100086, China)

⁴(School of Instrumentation Science and Opto-electronics Engineering, Beihang University, China)
(E-mail: xlwon@163.com)

In order to utilise the position and attitude information of a Celestial Navigation System (CNS) to aid a Strapdown Inertial Navigation System (SINS) and make it possible to achieve long-range and high-precision navigation, a new SINS/CNS integrated navigation scheme based on overall optimal correction is proposed. Firstly, the optimal installation angle of the star sensor is acquired according to the geometric relationship between the refraction stars area and the star sensor's visual field. Secondly, an analytical method to determine position and horizontal reference is introduced. Thirdly, the mathematical model of the SINS/CNS integrated navigation system is established. Finally, some simulations are carried out to compare the navigation performance of the proposed SINS/CNS integrated scheme with that of the traditional gyro-drift-corrected integration scheme. Simulation results indicate that in the proposed scheme, without the aid of SINS, CNS can provide attitude and position information and the errors of the SINS are able to be estimated and corrected efficiently. Therefore, the navigation performance of the proposed SINS/CNS scheme is superior to that of a more traditional scheme in long-range flight.

KEY WORDS

1. SINS. 2. CNS. 3. Integrated Navigation. 4. Overall Optimal Correction.

Submitted: 24 September 2016. Accepted: 28 April 2018. First published online: 12 July 2018.

1. INTRODUCTION. Today, High Altitude Long Endurance (HALE) Unmanned Aerial Vehicles (UAVs) are being widely used in both military and civilian domains due to advantages of low cost, zero casualty and so on. Since HALE UAVs are usually exposed to a complicated interference environment and are required to fly for a long time,

an autonomous and accurate long-endurance navigation system is urgently needed (Qu et al., 2011).

SINS has been widely used as a primary navigation system. However, due to the drifts and bias of Inertial Measurement Units (IMUs), a SINS cannot fully satisfy long-endurance and high-accuracy navigation demands. Therefore, some external information from other navigation systems must be introduced to aid SINS. This is called integrated navigation (Wang et al., 2013; 2012; Li et al., 2008). A Celestial Navigation System (CNS) can obtain both position and attitude information by observing celestial bodies via a star sensor (Ma et al., 2015). The errors of a CNS do not accumulate with time or distance. Therefore, the SINS/CNS integrated navigation scheme is an important development trend for autonomous long-endurance and long-range navigation (Yang and Wang, 2013).

When introducing CNS to assist SINS, it is crucial to obtain high precision horizon information which does not drift with time. At present, there are three methods to acquire horizontal reference information: the Inertial Navigation System (INS)-aided method (He et al., 2014), the direct horizon-sensing method and the indirect horizon-sensing method (Ning et al., 2013).

1.1. *INS-aided horizon-sensing method.* This method is usually applied to traditional SINS/CNS integrated navigation systems and is also called the gyro-drift-corrected integrated scheme. Generally, as CNS is measuring in inertial coordinates, attitude information should be converted to navigation coordinates before data fusion. This conversion depends on the horizontal information provided by SINS. Gyroscope drifts and attitude errors can be estimated, and navigation accuracy can be improved to a certain degree (Wang et al., 2012). However, the attitude conversion is based on the horizontal reference provided by SINS. Consequently, errors of SINS are introduced to the CNS, which will lead to attitude, position and velocity divergence in long-range flight.

1.2. *Direct horizon-sensing method.* CNS can acquire navigation star vectors and a geocentric vector by star sensor and infrared horizon sensor. Based on the two measurements, geometric relations, combined with orbital dynamics models and a filtering method, accurate speed and position information are easy to acquire (Ning et al., 2013). It is superior to the INS-aided horizon-sensing method in navigation accuracy (Wu and Wang, 2011). However, there are two drawbacks to this method. First, due to the irregularity of the Earth's surface and the low precision of infrared horizon sensors, measurement accuracy cannot be guaranteed for a long period. Secondly, nonlinear filtering and orbital dynamics models are necessary in the method.

1.3. *Indirect horizon-sensing method.* Unlike the two methods mentioned above, the indirect method makes use of refracted starlight and an astronomical refraction model to acquire a precise horizontal reference without the aid of SINS or other sensors. In addition, this method can provide accurate position information based on the dynamics model, measurements of the star sensor and atmospheric refraction model via nonlinear filtering (Ning et al., 2013). Currently, with the advent of star sensors with a large Field-Of-View (FOV), it is possible to observe multiple starlight vectors at the same time. Therefore, it is possible to obtain attitude and position information synchronously. Compared with traditional double-star sensors, large FOV star sensors have advantages such as: small volume, low cost, light weight and high accuracy (Qian et al., 2014; Zhang and Zhang, 2009; Quan and Fang, 2012).

However, when applying the third method to HALE UAVs, there are some limitations. First, when there is only a single star sensor, the star sensor installation will directly

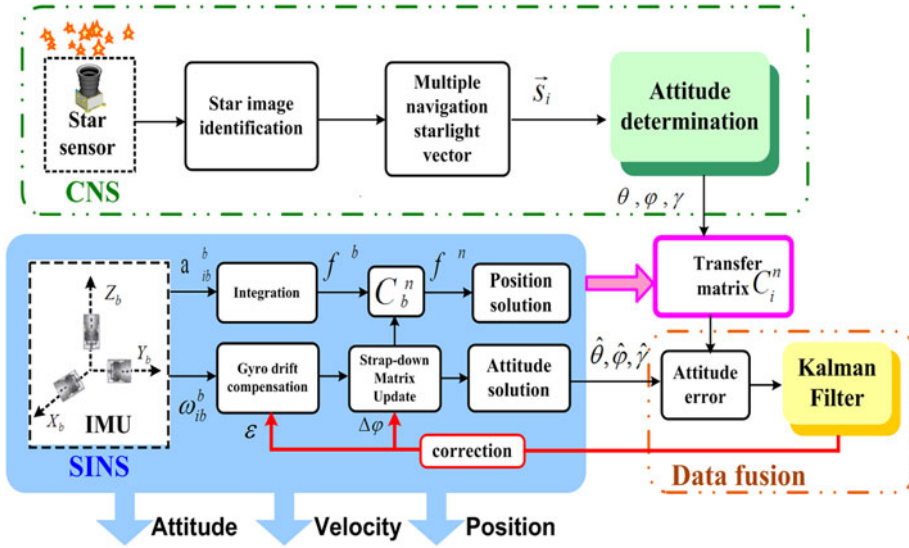


Figure 1. Schematic diagram of a gyro-drift-corrected SINS/CNS integrated navigation scheme.

influence the observations of the navigation and refraction stars, which will affect the accuracy of attitude and position determination. Thus, it is necessary to find a suitable installation angle. Secondly, the common SINS/CNS integrated navigation system based on stellar refraction is usually applied to Earth satellites and relies on the orbital dynamics models. However, the motion characteristics of a HALE UAV do not satisfy dynamic orbit models. Therefore, other positioning methods should be considered.

Consequently, in order to solve the limitations above, we propose a high-accuracy SINS/CNS integrated navigation scheme based on overall optimal correction. The paper consists of six sections. After this introduction, the SINS/CNS navigation scheme is described in Section 2. Position and attitude determination algorithms are explained in Section 3. In Section 4, the system model and measurement model of SINS/CNS are deduced. Simulation results are shown in Section 5 and conclusions are drawn in Section 6.

2. SINS/CNS INTEGRATED NAVIGATION SCHEME DESIGN.

2.1. *Scheme Design.* At present, most of the traditional SINS/CNS integrated navigation schemes are based on the gyro-drift-corrected mode, whose working principle is shown in Figure 1 (Hong et al., 2010; He et al., 2014).

CNS can obtain attitude according to the navigation star vector’s inertial frame, while SINS would provide the auxiliary matrix information C^n_i to convert the attitude to the navigation frame. The differences of attitude between CNS and SINS are then sent to the filter for data fusion. Misalignment angles and gyroscope drifts can be estimated and corrected effectively. However, on one hand, the navigation errors of SINS have been introduced into the transfer matrix C^n_i and on the other hand, due to the bias of the accelerometer, position errors will gradually accumulate and cannot be compensated. This results in a slow divergence in the navigation solution with time. Obviously, this kind of scheme cannot meet the requirements of long-endurance and high-accuracy navigation.

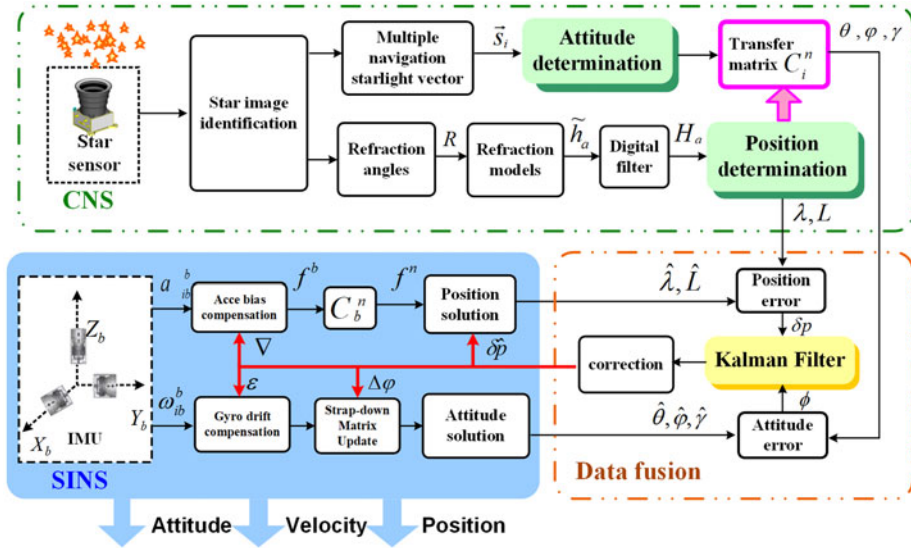


Figure 2. Schematic diagram of the proposed SINS/CNS integrated navigation scheme.

In order to improve the performance of the integrated navigation system mentioned above, a SINS/CNS integrated navigation scheme based on overall optimal correction is proposed for a HALE UAV. The integrated navigation scheme is composed of three parts: SINS subsystem, CNS subsystem and data fusion subsystem, as shown in Figure 2.

In the SINS subsystem, outputs of the IMU include angular rate ω_{lib}^b and specific force $f_{lib}^b \cdot \omega_{lib}^b$ and f_{lib}^b are used to calculate the position $\hat{\lambda}, \hat{L}, \hat{h}$, velocity \hat{v} and attitude $\hat{\theta}, \hat{\varphi}, \hat{\gamma}$ via the navigation solution mode. As the large FOV star sensor can observe multiple starlight vectors simultaneously, it is convenient to capture navigation stars and refraction stars. Navigation star vectors can be used to solve attitude θ, φ, γ . Apparent height \tilde{h}_a , which is used to calculate position λ, L, h , can be acquired by refraction stars and a stellar refraction model. As the observing noise of \tilde{h}_a cannot be neglected, a digital filter is introduced to pre-process the measurement \tilde{h}_a to improve the accuracy of positioning. The CNS will also provide the horizontal reference C_i^n , which is important for attitude conversion. The Kalman filter is then used for data fusion and measurements of the Kalman filter include attitude difference φ and position difference δ_p (Zhang et al., 2014). Finally, misalignment angles $\Delta\varphi$, position errors $\delta_{\hat{p}}$ and drifts of gyroscopes and bias of accelerometers can be estimated and corrected efficiently. Estimated states are then chosen to feed back so that the errors of SINS can be compensated efficiently (Quan et al., 2008).

Comparing the two schemes above, it is clear that the proposed integrated navigation system based on overall optimal correction has advantages as follows:

- (1) CNS can provide comprehensive independent navigation information. For the traditional gyro-drift-corrected scheme, CNS can only provide attitude information, while in the proposed scheme, CNS can output attitude, position and horizon references independently.
- (2) CNS is not constrained by the errors of SINS. In the traditional navigation scheme, star sensor measurement error, centroid extraction error and pattern matching error

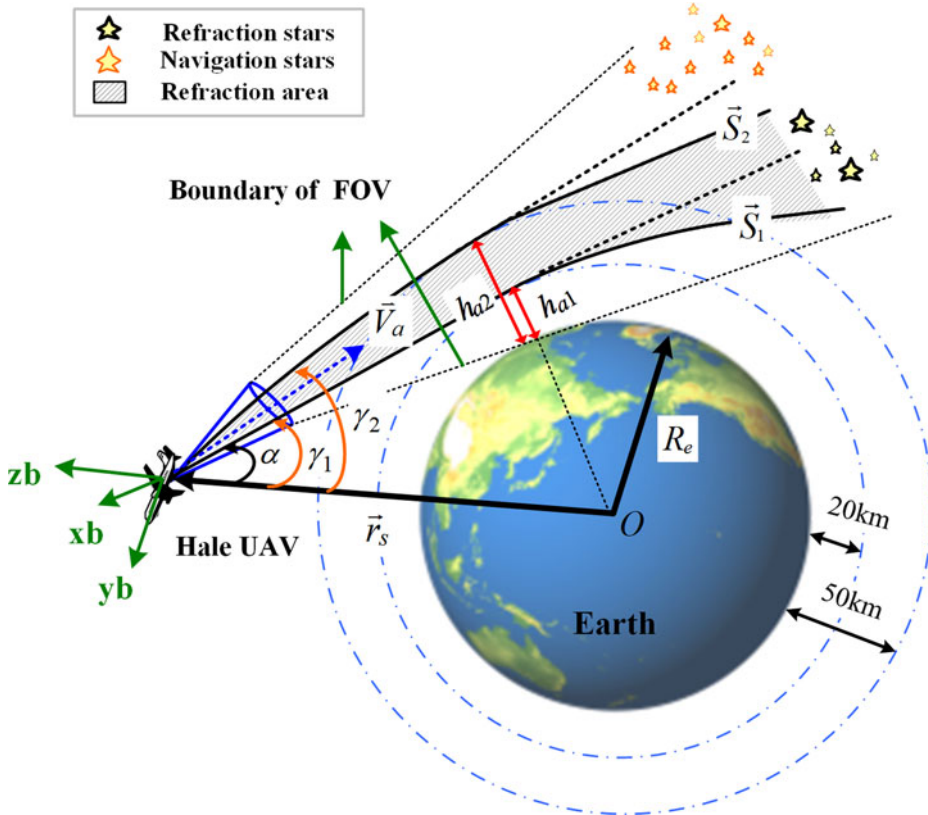


Figure 3. Diagrammatic sketch of the installation angle.

(Wang et al., 2012) are introduced, and SINS error is also included. However, in the proposed scheme, regardless of attitude or position determination, CNS is free from the influence of SINS errors. The reduction error sources can effectively slow down the divergence trend, which is more suitable for long-endurance navigation.

- (3) The errors of SINS can be estimated and corrected more comprehensively. In the traditional scheme, only misalignment angles and the gyro constant drifts can be estimated. In the proposed method, excepting misalignment angles and gyro drifts, position and velocity errors and accelerometer bias can be effectively estimated and compensated. Consequently, the navigation accuracy of the proposed scheme has been greatly improved.

2.2. Installation angle design. The large FOV star sensor is required to observe two kinds of starlight: one is navigation starlight, which is used for attitude determination and the other is refraction starlight, which is essential for calculating position. Obviously, installation angle and direction of optical axis are important factors, which will affect the observation results and then affect the accuracy of attitude and position. Therefore, it is necessary to find a reasonable installation angle.

As shown in Figure 3, the refraction area consists of two blue dotted circles and the two black dotted lines are the boundary of the FOV. Installation angle α is the included angle

between the negative direction of position vector $-\vec{r}_s$ and the optical axis direction vector \vec{V}_b . Generally, it is better to make the optical axis \vec{V}_b point to the refraction area, so that refraction stars can fall within the scope of the FOV to the greatest degree. By taking all the factors that may affect the accuracy of the atmospheric refraction model into consideration, we choose refracted height h_g ranging from $h_{g1} = 20$ km to $h_{g2} = 25$ km (Yang et al., 2015).

The critical refracted starlight \vec{S}_1 and \vec{S}_2 , at the height of h_{g1} , h_{g2} , are shown in Figure 3. The critical refraction angles R_1 and R_2 will be acquired by the empirical formula:

$$\begin{cases} R_1 = 6965.4793 e^{-0.15180263 h_{g1}} \\ R_2 = 6965.4793 e^{-0.15180263 h_{g2}} \end{cases} \tag{1}$$

Angle γ is defined as the included angle between position vector \vec{r}_s and refracted starlight vector \vec{S} and it can be calculated by the following formula:

$$\gamma = \arccos \left(\frac{\vec{r}_s \cdot \vec{S}}{|\vec{r}_s|} \right) \tag{2}$$

where $r_s = |\vec{r}_s|$ is the geocentric distance and R_e is the Earth’s radius.

According to Equation (1), the value range of γ can be acquired as follows:

$$\begin{cases} \gamma_1 \leq \gamma \leq \gamma_2 \\ \gamma_1 = \arcsin \left(\frac{R_e + h_{a1}}{r_s} \right) \\ \gamma_2 = \arcsin \left(\frac{R_e + h_{a2}}{r_s} \right) \end{cases} \tag{3}$$

The direction of the star sensor’s optical axis \vec{V}_b can be adjusted by installation angle α . If \vec{V}_b is located in the shadow area formed by critical refracted starlight \vec{S}_1 and \vec{S}_2 , there are a large number of refraction stars which can be captured by the star sensor. Therefore, it is necessary to find a reasonable installation angle α .

Figure 4 illustrates the geometric relationship of Figure 3 when projected onto the celestial sphere. Once the position of the HALE UAV M is acquired, its projection M' is as shown in Figure 4. If the refraction area 20 km–50 km is projected onto the celestial sphere, it would generate an annular area on the surface of the sphere, just as the blue annular shown in Figure 4. The red circle is the projection of the star sensor’s FOV and optical axis vector \vec{V} intersecting with the spherical surface at point V' which is the centre point of the red circle. The red circle has an overlapping part with a blue annular area, just as the hatched region $ABCD$ shown in Figure 4. Stars located in this area are refraction stars which can be observed by the star sensor. Since the area of $ABCD$ is decided by installation angle α , when the area value S_{ABCD} reaches its maximum, installation angle α is optimal for observing refraction stars. However, the value of S_{ABCD} can be reflected by included angle β between $\widehat{DM'}$ and $\widehat{VM'}$. Obviously, when the angle β achieves its maximum, installation angle α is correspondingly optimal.

As shown in Figure 4, $\widehat{AM'}$ and $\widehat{DM'}$ are both large arcs. According to the definition of the blue annulus, $\widehat{AM'} = \gamma_1$ and $\widehat{DM'} = \gamma_2$. Since $\widehat{DV'}$ is the radius of the red circle,

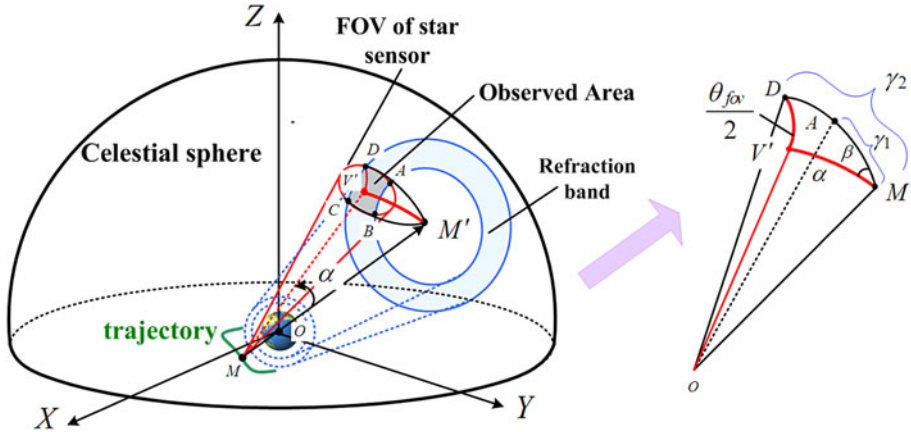


Figure 4. Geometric sketch of the installation angle in the celestial sphere.

the angular distance is $\theta_{fov}/2$. In the spherical triangle $M'DV'$, according to the cosine law of a spherical triangle, the following equation is formulated:

$$\cos \frac{\theta_{fov}}{2} = \cos a \cos \gamma_2 + \sin \alpha \sin \gamma_2 \cos \beta \tag{4}$$

where θ_{fov} is the FOV of the star sensor, α is the installation angle and β is the included angle between $\widehat{DM'}$ and $\widehat{V'M'}$. Then angle β can be determined:

$$\beta = \arccos \left\{ \frac{\cos \frac{\theta_{fov}}{2} - \cos \alpha \cos \gamma_2}{\sin \alpha \sin \gamma_2} \right\} \tag{5}$$

The differential of Equation (5) is written as:

$$\beta' = \frac{\left(\cos \frac{\theta_{fov}}{2} \cos \alpha - \cos \gamma_2 \right) \sin \gamma_2}{(\sin \alpha \sin \gamma_2)^2 \sqrt{1 - \left(\frac{\cos \frac{\theta_{fov}}{2} - \cos \alpha \cos \gamma_2}{\sin \alpha \sin \gamma_2} \right)^2}} \tag{6}$$

When $\beta' = 0$, the value of α is:

$$\alpha = \arccos \left(\frac{\cos \gamma_2}{\cos \frac{\theta_{fov}}{2}} \right) \tag{7}$$

From Equations (3) and (7), it can be summarised that the optimal installation angle is decided by the FOV of the star sensor θ_{fov} , refracted height h_g and position of the HALE UAV \vec{r}_s .

It is clear that, when the star sensor and refracted height are selected, θ_{fov} and h_g are constants. So, the installation angle α varies with position information \vec{r}_s . However, the installation angle of the star sensor cannot be changed. In order to make it possible to point the optical axis to the designated area, an attitude manoeuvre method is introduced. When

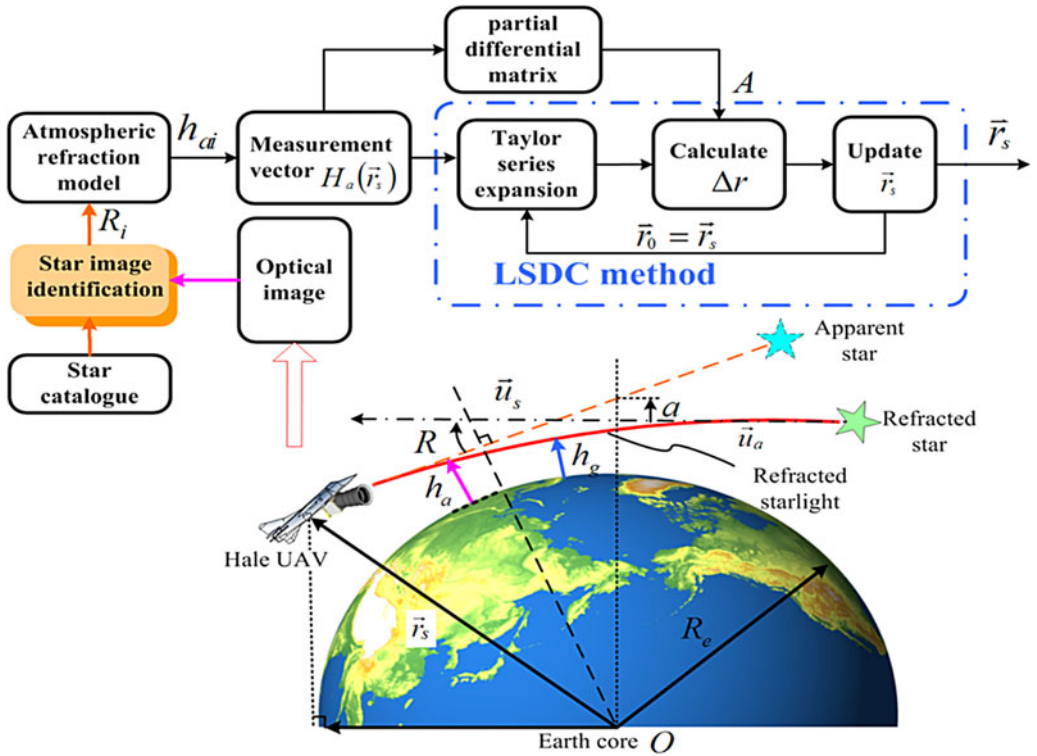


Figure 5. Schematic diagram of position determination algorithm.

a HALE UAV is flying for a long time, the navigation computer can provide navigation parameters and calculate attitude control commands in real time. Then the UAV will rotate around the centre of mass according to the attitude control commands to ensure the optical axis points to the best area. In addition, this ensures that there are enough refracted stars captured in the FOV of the star sensor.

3. ATTITUDE AND POSITION DETERMINATION ALGORITHM. In this paper, the key point of the SINS/CNS integrated navigation scheme is that the CNS can make use of the star sensor to determine attitude, position and horizontal references at the same time. The attitude determination method has been applied to actual flight missions (Hong et al., 2010). The traditional stellar refraction positioning method relies on an orbital dynamics model and a non-linear filter (Ma et al., 2015). However, the motion characteristics of a HALE UAV do not satisfy the orbital dynamics equation. To solve this problem, a position method based on the least square differential correction is introduced (Wang and Ma, 2009).

3.1. Position and horizontal reference determination algorithm. The density of the atmosphere is uneven. Consequently, when starlight passes through the atmosphere, it will be refracted and then bend gradually towards the centre of the Earth. Therefore, viewed from a HALE UAV, the position of an apparent star will be higher than that of the actual star. Apparent ray \vec{u}_a diverges from actual ray \vec{u}_s as shown in Figure 5. Angle R between \vec{u}_a and \vec{u}_s is defined as the refraction angle. According to Figure 5, the refracted ray appears

to graze the horizon of the Earth at an apparent height h_a , but is actually at a slightly lower height h_g . There is a nonlinear mathematical relation between apparent height h_a and position vector \vec{r}_s .

In order to acquire position information, it is necessary to solve nonlinear equations. The Least Square Differential Correction (LSDC) method, which is efficient in dealing with the nonlinear measurement, is introduced in this paper. Figure 5 illustrates the process of position determination based on LSDC. It includes the following six steps:

Step 1. Acquire refraction angle R. Firstly, it is necessary to obtain the refraction angle R . After star image identification (Wang et al., 2012), the position of a refraction star in measuring frame (s) can be denoted as \vec{S}_{rs} :

$$\vec{S}_{rs} = \frac{1}{\sqrt{(x_r - x_0)^2 + (y_r - y_0)^2 + f^2}} \begin{bmatrix} -(x_r - x_0) \\ -(y_r - y_0) \\ f \end{bmatrix} \tag{8}$$

where (x_r, y_r) is the centre point of this refraction star in the (s) frame, (x_0, y_0) is the centre point of the lens in the (s) frame and f is the focal length of the star sensor.

The actual position of the star in the (i) frame is \vec{S}_i , which can be obtained by reference to a star catalogue after star image identification. Then, combined with installation matrix C_s^b and attitude matrix C_i^b , vector \vec{S}_i can be transformed into the (s) frame as Equation (9) shows:

$$\vec{S}_{is} = (C_s^b)^T C_i^b \vec{S}_i \tag{9}$$

Therefore, based on the definition of refraction angle R , R can be determined by the following equation:

$$R = \arccos \left(\left(\vec{S}_{rs} \right)^T \vec{S}_{is} \right) \tag{10}$$

Step 2. Construct measurement matrix H_a . There is an accurate function describing the relationship between refraction angle R and refraction height h_g (Yang et al., 2014):

$$h_g = h_0 - H \ln(R) + H \ln(\rho_0) + H \ln \left(k(\lambda) \sqrt{\frac{2\pi R_e}{H}} \right) \tag{11}$$

where h_0 is a reference height; $k(\lambda)$ is the scattering coefficient; R_e is Earth’s radius; ρ_0 is the atmospheric density at height of h_0 and H is the atmospheric density scale height.

Assuming that the atmosphere satisfies spherical lamination, according to the optical refraction law, refraction height h_g and apparent height h_a have the following relationship:

$$h_a = h_g + (R_e + h_g) \cdot \sqrt{\frac{H}{2\pi R_e}} \tag{12}$$

Associating Equation (11) with Equation (12) and taking $R_e \gg h_a$ into consideration, it is easy to deduce the mathematical formula between h_a and R :

$$h_a = h_0 - H \ln(R) + H \ln(\rho_0) + H \ln \left(k(\lambda) \sqrt{\frac{2\pi R_e}{H}} \right) + R \sqrt{\frac{HR_e}{2\pi}} \tag{13}$$

where $H, \rho_0, h_0, R_e, k(\lambda)$ are all constant when λ is given. Once a refraction angle is acquired, corresponding height h_a is also derived via Equation (13).

As is shown in Figure 5, apparent height h_a , refraction angle R , and the UAV's geocentric distance r_s satisfy the following equation:

$$h_a = \sqrt{r_s^2 - u^2} + u \tan(R) - R_e - a \tag{14}$$

where \vec{r}_s is the position vector and $\vec{u}_s = [\cos \delta_s \cos \alpha_s, \cos \delta_s \sin \alpha_s, \sin \delta_s]^T$ is the unit position vector of the refraction star in the (i) frame. δ_s is declination and α_s is right ascension. $u = |\vec{r}_s \cdot \vec{u}_s|$ and a is a small constant as shown in Figure 5 and is usually neglected when calculating h_a . When starlight is close to the surface of the Earth, the refraction will become more obvious. So, refraction of starlight mainly occurs in the stratosphere and troposphere. Refracted starlight observed from the top of the stratosphere is little different to that observed from outside the atmosphere (Hays and Roble, 1967). According to Equations (13) and (14), the positioning error caused by the refraction angle is about 134.93 m when the measuring error of the star sensor is 3'' and its height is 30 km. Therefore, if the accuracy of the star sensor is high enough, the influence of the refraction angle on positioning accuracy can be controlled in a very small range. So, as long as a HALE UAV is flying beyond the stratosphere (more than 30 km), the traditional star refraction model is still available.

We assume that there are n ($n \geq 3$) refraction stars which are captured by the star sensor. According to Equation (7), refraction angles $[R_1, R_2 \dots R_n]^T$ can be acquired. Based on Equation (14), measurement vector $H_a(\vec{r}_s)$ is also acquired:

$$H_a(\vec{r}_s) = \begin{bmatrix} h_{a1} \\ h_{a2} \\ \vdots \\ h_{an} \end{bmatrix} = \begin{bmatrix} \sqrt{r_s^2 - u_1^2} + u_1 \tan(R_1) - R_e \\ \sqrt{r_s^2 - u_2^2} + u_2 \tan(R_2) - R_e \\ \vdots \\ \sqrt{r_s^2 - u_n^2} + u_n \tan(R_n) - R_e \end{bmatrix} \tag{15}$$

where h_{ai} is the apparent height of the i th refraction star; $\vec{r}_s = [r_x \ r_y \ r_z]^T$ is the position vector of the HALE UAV; $\vec{u}_{Si} = [\cos \delta_{Si} \cos \alpha_{Si}, \cos \delta_{Si} \sin \alpha_{Si}, \sin \delta_{Si}]^T$ is the unit position vector of the i -th star in the (i) frame and $u_i = |\vec{r}_s \cdot \vec{u}_{Si}|$ ($i = (1, 2, \dots, n)$). Equation (15) is an equation with three unknown quantities r_x, r_y, r_z .

Step 3. Solve position \vec{r}_s based on measurement vector H_a . We choose \vec{r}_{s0} as the initial value of position vector \vec{r}_s and the first-order Taylor series expansion of Equation (15) at the point of \vec{r}_{s0} is expressed as:

$$H_a(\vec{r}_s) = H_a(\vec{r}_{s0}) + A \cdot \Delta \vec{r} + V \tag{16}$$

where V is the residual sequence of the first order Taylor expansion of Equation (16); $\Delta \vec{r} = \vec{r}_s - \vec{r}_{s0}$ is the differential correction and A is the partial derivative matrix of $H_a(\vec{r}_s)$

with respect to the position vector \vec{r}_s . It can be calculated by the following formula:

$$A = \frac{\partial H_a(r_s)}{\partial r_s} = \begin{bmatrix} \frac{\partial h_{a1}}{r_x} & \frac{\partial h_{a1}}{r_y} & \frac{\partial h_{a1}}{r_z} \\ \frac{\partial h_{a2}}{r_x} & \frac{\partial h_{a2}}{r_y} & \frac{\partial h_{a2}}{r_z} \\ \vdots & \vdots & \vdots \\ \frac{\partial h_{an}}{r_x} & \frac{\partial h_{an}}{r_y} & \frac{\partial h_{an}}{r_z} \end{bmatrix} \tag{17}$$

$$\begin{cases} \frac{\partial h_{a_i}}{r_x} = \frac{r_x - u_i \cdot \cos \delta_i \cos \alpha_i}{\sqrt{r_s^2 - u_i^2}} \\ \frac{\partial h_{a_i}}{r_y} = \frac{r_y - u_i \cdot \cos \delta_i \sin \alpha_i}{\sqrt{r_s^2 - u_i^2}} \\ \frac{\partial h_{a_i}}{r_z} = \frac{r_z - u_i \cdot \sin \delta_i}{\sqrt{r_s^2 - u_i^2}} \end{cases} \quad (i = 1, 2, \dots, n) \tag{18}$$

Then the value of differential correction $\Delta \hat{r}$ can be acquired from the following equation:

$$\Delta \hat{r} = (A^T A)^{-1} A^T (H_a(\vec{r}_s) - H_a(\vec{r}_{s0})) \tag{19}$$

Updated \vec{r}_s with $\Delta \hat{r}$:

$$\vec{r}_{sc} = \vec{r}_{s0} + \Delta r \tag{20}$$

The process above is repeated by using the corrected \vec{r}_{sc} as the initial value \vec{r}_{s0} in the next turn until the difference between \vec{r}_{sc} and \vec{r}_{s0} satisfies the iteration termination requirement $|\vec{r}_{sc} - \vec{r}_{s0}| < \epsilon$. The solution of \vec{r}_s is \vec{r}_{s0} .

Since position vector $\vec{r}_s = [r_x \ r_y \ r_z]^T$ has been solved, it is convenient to calculate declination δ_d , right ascension α_d and height h of a HALE UAV in the (i) frame:

$$\begin{aligned} \alpha_d &= \arctan(r_y/r_x) \\ \delta_d &= \arctan\left(r_z/\sqrt{r_x^2 + r_y^2}\right) \\ h &= r_z - R_e \end{aligned} \tag{21}$$

where $\alpha_d \in (0 \sim 2\pi)$, $\delta_d \in (-\pi/2 \sim \pi/2)$. Then, declination δ_d and right ascension α_d can be transformed to the navigation frame (n) . Therefore, geographic latitude L and longitude λ can be written as:

$$\begin{aligned} \lambda &= \alpha_d - t_G \\ L &= \delta_d \end{aligned} \tag{22}$$

where t_G is the Greenwich Hour Angle (GHA) of the Spring Equinox.

Step 4. Extract horizontal reference. Position vector \vec{r}_s obtained in Step 3 can also be used to calculate matrix C_i^n since \vec{r}_s contains the horizontal information. \vec{p} represents the unit

position vector which can be expressed as:

$$\vec{p} = \vec{r}_s / |\vec{r}_s| = [p_x \ p_y \ p_z]^T \tag{23}$$

Matrix C_i^n can be derived by the following formula:

$$C_i^n = \begin{bmatrix} -\frac{p_y}{\sqrt{1-p_z^2}}, & \frac{p_x}{\sqrt{1-p_z^2}} & 0 \\ -\frac{p_x p_z}{\sqrt{1-p_z^2}} & -\frac{p_y p_z}{\sqrt{1-p_z^2}} & \sqrt{1-p_z^2} \\ p_x & p_y & p_z \end{bmatrix}^T \tag{24}$$

Up to now, position and horizontal references with high-accuracy have both been acquired via the least square differential correction method.

3.2. *Attitude determination algorithm.* Assuming that n ($n > 3$), navigation stars can be captured, and will generate an optical image on the Charge Coupled Device (CCD) surface. (x_{Si}, y_{Si}) is the centre point of the i -th navigation star in (s) frame. The i -th starlight vector can be formulated as:

$$S_{is} = \frac{1}{\sqrt{x_{Si}^2 + y_{Si}^2 + f^2}} \begin{bmatrix} x_{Si} \\ y_{Si} \\ -f \end{bmatrix}, \quad (i = 1, 2 \dots n) \tag{25}$$

where f is the focal length of the star sensor.

Multiple vectors of n ($n > 3$) stars in (s) frame are denoted as C_s . Position vectors of n stars C_i , in the (i) frame can be acquired by star image identification. According to the installation relationship between a star sensor and a HALE UAV, it is easy to calculate the installation matrix M_s^b . Then the attitude matrix A_b^i has the following relationship with C_s, C_i , and M_s^b :

$$c_i = A_b^i M_s^b C_s \tag{26}$$

Finally, the high precision attitude matrix A_b^i can be calculated by using the least squares method.

Equation (24) provides horizontal reference C_i^n and combined with A_b^i solved in Equation (26), it is easy to acquire matrix C_b^n which can be used to calculate attitude information:

$$C_b^n = C_i^n \cdot A_b^i \tag{27}$$

According to the definition of attitude angles, $[\varphi, \gamma, \psi]^T$ are derived by the following formula:

$$\begin{bmatrix} \varphi \\ \gamma \\ \psi \end{bmatrix} = \begin{bmatrix} \arcsin C_b^n(3, 2) \\ -\arctan[C_b^n(3, 1)/C_b^n(3, 3)] \\ \arctan[C_b^n(1, 2)/C_b^n(2, 2)] \end{bmatrix} \tag{28}$$

Based on the analysis above, it is summarised that the proposed SINS/CNS scheme relying on a single large FOV star sensor is able to provide real-time position, horizontal reference and attitude information for a HALE UAV. The positioning algorithm principle of a star sensor is simple with only a small amount of calculation. The horizontal reference is totally free from SINS, which results in a higher attitude precision.

4. MATHEMATICAL MODEL.

4.1. *System model.* We select the misalignment angles, velocity errors, position errors, drifts of gyroscopes and zero biases of accelerometers as system states. According to error equations of SINS, the system model is as below:

$$\dot{X} = FX + CW \tag{29}$$

where the state vector is $X = [\phi_x, \phi_y, \phi_z, \delta v_x, \delta v_y, \delta v_z, \delta L, \delta \lambda, \delta h, \varepsilon_x, \varepsilon_y, \varepsilon_z, \nabla_x, \nabla_y, \nabla_z]^T$, including misalignment angles ϕ_x, ϕ_y, ϕ_z , velocity errors $\delta v_x, \delta v_y, \delta v_z$, position errors $\delta L, \delta \lambda, \delta h$, gyroscope drifts $\varepsilon_x, \varepsilon_y, \varepsilon_z$ and accelerometers biases $\nabla_x, \nabla_y, \nabla_z$.

F is the state transition matrix:

$$F = \begin{bmatrix} F_{N(9 \times 9)} & F_{S(6 \times 6)} \\ 0_{(6 \times 9)} & 0_{(9 \times 6)} \end{bmatrix} \tag{30}$$

Non-zero elements of F_N are:

| | |
|--|--|
| $F_N(1, 2) = \omega_{ie} \sin L + \frac{v_x}{R_N + h} \tan L$ | $F_N(1, 3) = -\left(\omega_{ie} \cos L + \frac{v_x}{R_N + h}\right)$ |
| $F_N(1, 5) = -\frac{1}{R_M + h}$ | $F_N(2, 1) = -\left(\omega_{ie} \sin L + \frac{v_x}{R_N + h} \tan L\right)$ |
| $F_N(2, 3) = -\frac{v_y}{R_M + h}$ | $F_N(2, 4) = \frac{1}{R_N + h}$ |
| $F_N(2, 7) = -\omega_{ie} \sin L$ | $F_N(3, 1) = \omega_{ie} \cos L + \frac{v_x}{R_N + h}$ |
| $F_N(3, 2) = \frac{v_y}{R_M + h}$ | $F_N(3, 4) = \frac{1}{R_N + h} \tan L$ |
| $F_N(3, 7) = \omega_{ie} \cos L + \frac{v_x}{R_N + h} \sec^2 L$ | $F_N(4, 2) = -f_z$ |
| $F_N(4, 3) = f_y$ | $F_N(4, 4) = \frac{v_y}{R_M + h} \tan L - \frac{v_z}{R_M + h}$ |
| $F_N(4, 5) = 2\omega_{ie} \sin L + \frac{v_x}{R_N + h} \tan L$ | $F_N(4, 6) = -\left(2\omega_{ie} \cos L + \frac{v_x}{R_N + h}\right)$ |
| $F_N(4, 7) = 2\omega_{ie} v_y \cos L$ | $F_N(5, 1) = f_z$ |
| $+ \frac{v_x v_y}{R_N + h} \sec^2 L + 2\omega_{ie} v_z \sin L$ | $F_N(5, 4) = -2\left(\omega_{ie} \sin L + \frac{v_x}{R_N + h} \tan L\right)$ |
| $F_N(5, 3) = -f_x$ | $F_N(5, 6) = -\frac{v_y}{R_M + h}$ |
| $F_N(5, 5) = -\frac{v_z}{R_M + h}$ | $F_N(6, 1) = -f_y$ |
| $F_N(5, 7) = -2\left(\omega_{ie} \cos L + \frac{v_x}{R_N + h} \sec^2 L\right) v_x$ | $F_N(6, 4) = -2\left(\omega_{ie} \cos L + \frac{v_x}{R_N + h}\right)$ |
| $F_N(6, 2) = f_x$ | |

$$\begin{aligned}
 F_N(6, 5) &= \frac{2v_y}{R_M + h} & F_N(6, 7) &= -2\omega_{ie}v_x \sin L \\
 F_N(7, 5) &= \frac{1}{R_M + h} & F_N(8, 4) &= \frac{1}{R_N + h} \sec L \\
 F_N(8, 7) &= \frac{v_x}{R_N + h} \sec L \tan L & F_N(9, 6) &= 1
 \end{aligned}$$

where ω_{ie} is the rotational angular velocity of the Earth; v_x, v_y, v_z is the velocity provided by SINS; f_x, f_y, f_z is the specific force along the three axes; R_M is the main radius of curvature of the meridian and R_N is the main radius of curvature of prime vertical.

F_s can be expressed as:

$$F_s = \begin{bmatrix} -C_b^n & 0_{3 \times 3} \\ 0_{3 \times 3} & C_b^n \end{bmatrix} \tag{31}$$

G is the noise driven array:

$$G = \begin{bmatrix} -C_b^n & 0_{3 \times 3} \\ 0_{3 \times 3} & C_b^n \\ 0_{9 \times 3} & 0_{9 \times 3} \end{bmatrix} \tag{32}$$

$W = [\omega_{gx} \ \omega_{gy} \ \omega_{gz} \ \omega_{dx} \ \omega_{dy} \ \omega_{dz}]^T$ is the noise vector, where $\omega_{gx}, \omega_{gy}, \omega_{gz}$ is the noise of the gyroscope and $\omega_{dx}, \omega_{dy}, \omega_{dz}$ is the noise of the accelerometer along the three axes.

4.2. *Measurement model.* Misalignment angles and position errors are selected to be measurements of Kalman filter. The misalignment angle vector can be calculated from the attitude error of SINS and CNS. $\delta = [\delta\theta, \delta\varphi, \delta\gamma]$ stands for attitude error and according to its definition, it can be expressed as:

$$\begin{cases} \delta\theta = \hat{\theta} - \theta \\ \delta\varphi = \hat{\varphi} - \varphi \\ \delta\gamma = \hat{\gamma} - \gamma \end{cases} \tag{33}$$

where $\hat{\theta}, \hat{\varphi}, \hat{\gamma}$ is the attitude of SINS and θ, φ, γ is the attitude provided by CNS.

Assuming that \hat{C}_n^b is the attitude matrix calculated by SINS and the actual attitude matrix is C_n^b , these two matrices satisfy the following equation:

$$C_n^b = \hat{C}_n^b C_n^p = \begin{bmatrix} C_{11} & C_{12} & C_{13} \\ C_{21} & C_{22} & C_{23} \\ C_{31} & C_{32} & C_{33} \end{bmatrix} = \begin{bmatrix} \hat{C}_{11} & \hat{C}_{12} & \hat{C}_{13} \\ \hat{C}_{21} & \hat{C}_{22} & \hat{C}_{23} \\ \hat{C}_{31} & \hat{C}_{32} & \hat{C}_{33} \end{bmatrix} \begin{bmatrix} 1 & \phi_z & -\phi_y \\ -\phi_z & 1 & \phi_x \\ \phi_y & -\phi_x & 1 \end{bmatrix} \tag{34}$$

According to the identification of C_n^b , it is clear that $\sin \theta = C_{23}$, $\tan \varphi = C_{21}/C_{22}$ and $\tan \gamma = -C_{13}/C_{33}$. Referring to Equations (33) and (34), the following three equations are given as:

$$\sin(\hat{\theta} - \delta\theta) = -\phi_y \hat{C}_{21} + \phi_x \hat{C}_{22} + \hat{C}_{23} \tag{35}$$

$$\tan(\hat{\varphi} - \delta\varphi) = \frac{\hat{C}_{21} - \phi_z \hat{C}_{22} + \phi_y \hat{C}_{23}}{\phi_z \hat{C}_{21} + \hat{C}_{22} - \phi_x \hat{C}_{23}} \tag{36}$$

$$\tan(\hat{\gamma} - \delta\gamma) = -\frac{-\phi_y \hat{C}_{11} + \phi_x \hat{C}_{12} + \hat{C}_{13}}{-\phi_y \hat{C}_{31} + \phi_x \hat{C}_{32} + \hat{C}_{33}} \tag{37}$$

We linearize the left parts of Equations (35), (36) and (37) and expand the right parts of Equation (35), (36) and (37) using the Taylor series. Equations (35), (36) and (37) can be transformed as the following three equations, when neglecting the second-order or more than second-order small quantity:

$$\delta\theta = -\phi_x \cos \hat{\varphi} + \phi_y \sin \hat{\varphi} \tag{38}$$

$$\delta\varphi = -\phi_x \sin \hat{\varphi} \tan \hat{\theta} - \phi_y \cos \hat{\varphi} \tan \hat{\theta} + \phi_z \tag{39}$$

$$\delta\gamma = -\phi_x \frac{\sin \hat{\varphi}}{\cos \hat{\theta}} - \phi_y \frac{\cos \hat{\varphi}}{\cos \hat{\theta}} \tag{40}$$

Therefore, the misalignment angles ϕ_x, ϕ_y, ϕ_z can be determined by attitude error:

$$\begin{bmatrix} \phi_x \\ \phi_y \\ \phi_z \end{bmatrix} = \begin{bmatrix} -\cos \hat{\varphi} & 0 & -\sin \hat{\varphi} \cos \hat{\theta} \\ \sin \hat{\varphi} & 0 & -\cos \hat{\varphi} \cos \hat{\theta} \\ 0 & 1 & -\sin \hat{\theta} \end{bmatrix} \begin{bmatrix} \delta\theta \\ \delta\varphi \\ \delta\gamma \end{bmatrix} \tag{41}$$

Then the measurement equation can be expressed as:

$$Z_1 = H_1 X + V_1 \tag{42}$$

where $Z_1 = [\phi_x \ \phi_y \ \phi_z]^T$; $H_1 = [I_{3 \times 3} \ 0_{3 \times 12}]$ is the measuring vector and V_1 stands for measuring noise.

When the measurement is the position error between SINS and CNS, the measurement equation can be expressed as:

$$Z_2 = H_2 X + V_2 \tag{43}$$

where $Z_2 = [\hat{L} - L \ \hat{\lambda} - \lambda]^T$ is the position error; $\hat{L}, \hat{\lambda}$ and L, λ are the position results provided by SINS and CNS; $H_2 = [0_{2 \times 6} \ I_{2 \times 2} \ 0_{2 \times 7}]$ is the corresponding measurement vector and V_2 is measuring noise.

Therefore, based on Equations (42) and (43), the measurement model of SINS/CNS integrated navigation system is deduced as:

$$Z = HX + V \tag{44}$$

where $Z = [Z_1 \ Z_2]^T$; $H = [H_1 \ H_2]^T$; $V = [V_1 \ V_2]^T$.

Finally, the state model Equation (29) and the measurement model Equation (44) are linear, and a Kalman filter is utilised to estimate the state to correct the errors of SINS.

5. SIMULATION VERIFICATION AND ANALYSIS.

5.1. *Simulation conditions.* The simulation conditions are as follows (Wu et al., 2006). Table 1 shows the initial navigation parameters and Table 2 gives the bias, drifts and noise of the related measuring devices. Table 3 sets the simulation time.

Based on the simulation conditions above, a UAV flight simulation scenario of four hours was designed and is illustrated in Figure 6. It includes all the motion patterns of the UAV, such as straight-line motion, turning motion, acceleration, deceleration, climbing and descending.

Table 1. Initial navigation parameters.

| | |
|------------------------|---|
| Initial position | $\mathbf{P}_0 = [40^\circ\text{N}, 100^\circ\text{E}, 30 \text{ km}]^T$ |
| Initial position error | $\Delta\mathbf{P}_0 = [100 \text{ m}, 100 \text{ m}, 200 \text{ m}]^T$ |
| Initial velocity | $\mathbf{V}_0 = [141.4 \text{ m/s}, 141.4 \text{ m/s}, 0]^T$ |
| Initial velocity error | $\Delta\mathbf{V}_0 = [0.2 \text{ m/s}, 0.2 \text{ m/s}, 0]^T$ |
| Initial attitude | $\boldsymbol{\varphi}_0 = [0^\circ, 0^\circ, 0^\circ]^T$ |
| Initial attitude error | $\Delta\boldsymbol{\varphi}_0 = [10'', 10'', 60'']^T$ |

Table 2. Bias, drift and noise of measuring devices.

| | |
|----------------------------------|--|
| Bias of accelerometer | $\boldsymbol{\epsilon} = [10 \mu\text{g}, 10 \mu\text{g}, 10 \mu\text{g}]^T$ |
| Measuring noise of accelerometer | $\boldsymbol{\omega}_d = [5 \mu\text{g}, 5 \mu\text{g}, 5 \mu\text{g}]^T$ |
| Constant drift of groscope | $\Delta = [0.01^\circ/\text{h}, 0.01^\circ/\text{h}, 0.01^\circ/\text{h}]^T$ |
| Measuring noise of groscope | $\boldsymbol{\omega}_g = [0.005^\circ/\text{h}, 0.005^\circ/\text{h}, 0.005^\circ/\text{h}]^T$ |
| Measuring noise of star sensor | $\boldsymbol{\omega}_s = 3''$ |
| Accuracy of radar altimeter | $\mathbf{R}_a = 5 \text{ m}$ |

Table 3. Simulation time.

| | |
|-----------------------|-------------------------|
| Total simulation time | $T_{a11} = 4 \text{ h}$ |
| Sampling time of SINS | $t_s = 0.02 \text{ s}$ |
| Sampling time of CNS | $t_c = 1 \text{ s}$ |
| Kalman filter period | $T = 1 \text{ s}$ |

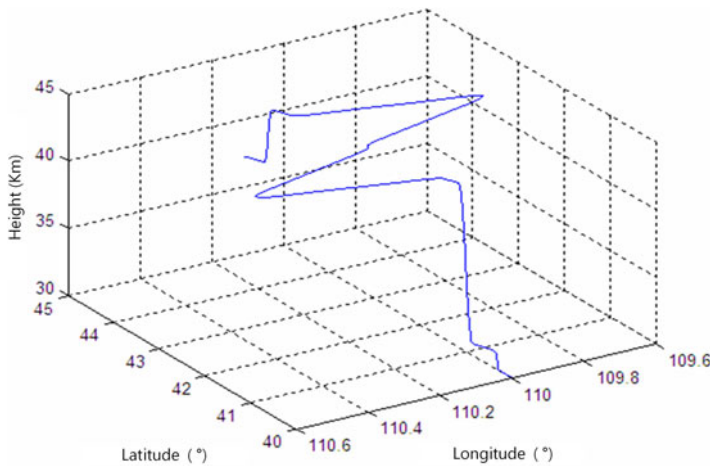


Figure 6. Simulated four hour HALE UAV trajectory.

5.2. Simulation results and analysis.

5.2.1. Number of visible navigation and refraction stars. It is necessary to analyse the number of stars when a HALE UAV is flying for a long time. First, we exclude binary stars, variable stars and the stars whose magnitude is greater than 6.5 in the Tycho2 catalogue (Høg et al., 2000), and a simplified whole-sky star catalogue can be determined. The FOV of the star sensor is $20^\circ \times 20^\circ$, and the resolution of the image plane is defined as $N_x \times$

Table 4. Statistical table of number of stars screened by star sensor in one hour.

| Type | $N_n \geq 3$ | $N_r = 0$ | $N_r \geq 3$ | $N_r \geq 30$ |
|------------|--------------|-----------|--------------|---------------|
| Times | 3600 | 211 | 2998 | 2720 |
| Proportion | 100% | 5.86% | 83.28% | 75.56% |

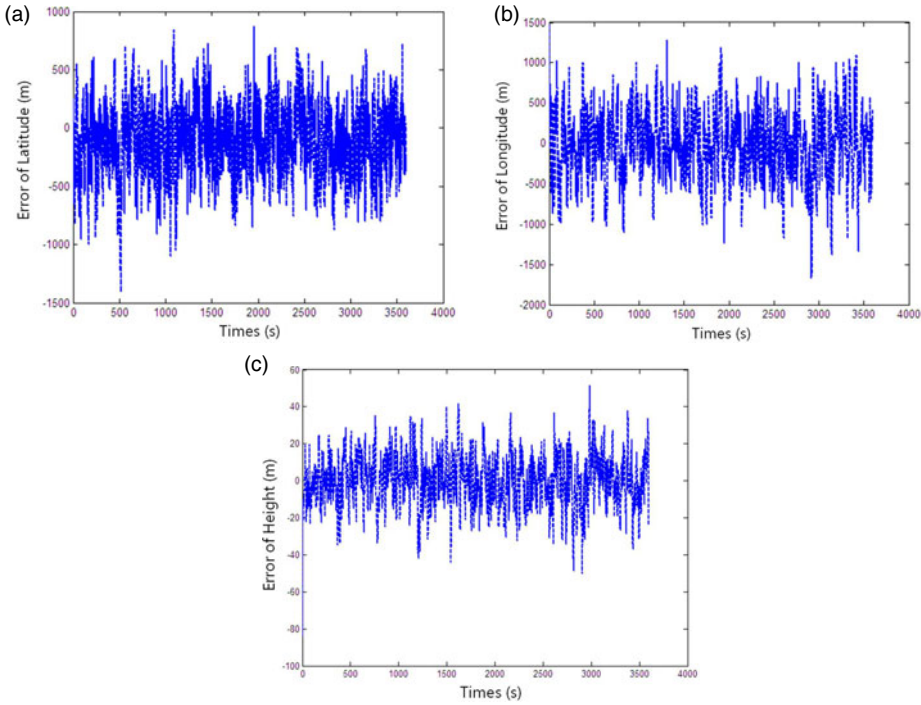


Figure 7. Position error of pure celestial analytic position algorithm.

$N_y = 1024 \times 1024$. Pixel size is $14.7 \mu\text{m}$. The total observing time is one hour, and the interval time is set as 1 s. The number navigation stars and refraction stars screened by the star sensor in one hour is shown in Table 4. N_n stands for the number of navigation stars and N_r stands for the number of refraction stars.

It can be seen clearly from Table 4, that over the whole hour, there are always more than three navigation stars in the FOV of the star sensor. This means that the attitude determination procedure can be carried out successfully. On only a few occasions (5.86% of total time) does the star sensor fail to capture refraction stars. However, during 83.28% of the whole period, the number of refraction stars is more than three. So, we contend that the proposed pure analytic positioning algorithm based on stellar refraction is feasible.

5.3. *System performance verification and analysis.* Based on the information above, the performance of the analytical positioning method is verified. We select the variance of refracted height noise as 80 m when there are more than three refraction stars, and the CNS can update the position of the UAV. While there are less than three refraction stars, CNS uses the positioning results at the last good fix. Simulation positioning results are shown in Figure 7. Results show that the proposed pure celestial analytic positioning algorithm is

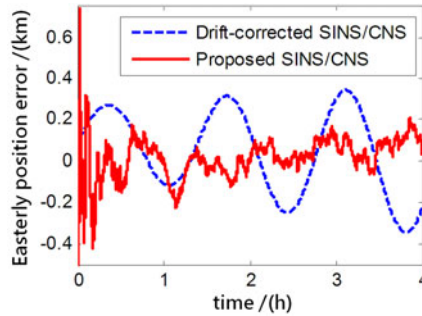


Figure 8. Easterly position error.

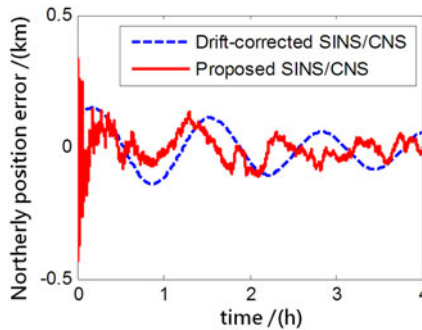


Figure 9. Northerly position error.

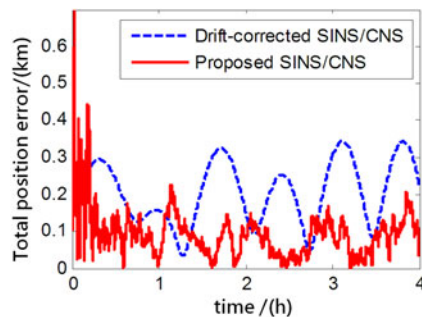


Figure 10. Total position error.

feasible. When the HALE UAV is flying for one hour, latitude error is maintained at about 500 m and longitude error does not exceed 1,000 m. The maximum height error is less than 60 m.

The performance of the proposed SINS/CNS integrated navigation system are compared with that of a traditional gyro-drift-corrected SINS/CNS integrated system, as shown in Figures 8–16. In order to distinguish different simulation results of the two integration schemes, red curves are used to express the results of the proposed navigation scheme and blue curves illustrate the results of the traditional gyro-drift-corrected SINS/CNS scheme.

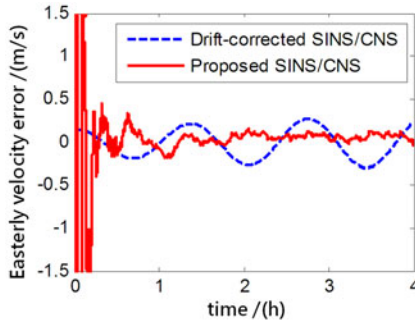


Figure 11. Easterly velocity error.

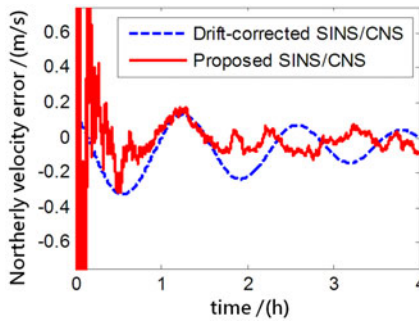


Figure 12. Northerly velocity error.

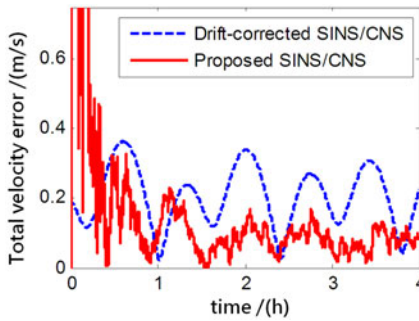


Figure 13. Total velocity error.

Figures 8–10 illustrate the position errors of the proposed SINS/CNS scheme and the drift-corrected SINS/CNS scheme. Figures 11–13 compare the velocity error, and attitude error is shown in Figures 14–16. Table 5 shows the performance precision comparison between the gyro-drift-corrected SINS/CNS scheme and the proposed scheme (including variance and maximum value of navigation error).

As the blue curves show in Figures 8–10, the position errors of the gyro-drift-corrected SINS/CNS scheme are gradually diverging with time and the maximum total position error reaching 343.20 m, as shown in Table 5. However, as shown in the red curves, it is clear that the position errors of the proposed SINS/CNS scheme are sharply reduced. With the

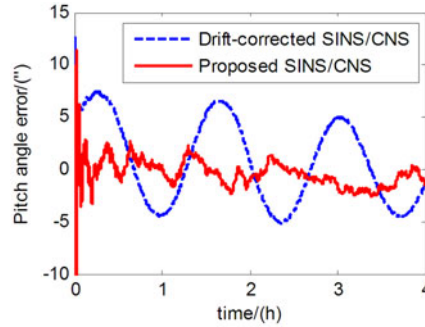


Figure 14. Pitch angle error.

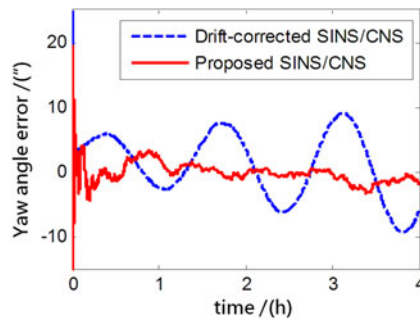


Figure 15. Yaw angle error.

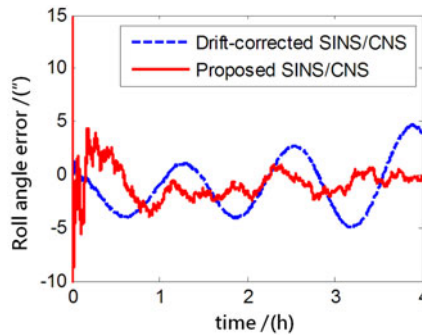


Figure 16. Roll angle error.

aid of CNS, the maximum total position error is reduced to 208.75 m. Velocity accuracy of the proposed scheme is also improved as shown in the curves in Figures 11–13. Compared with the gyro-drift-corrected scheme, velocity error of the proposed scheme does not diverge, and the maximum error is reduced from 0.363 m/s to 0.168 m/s, as shown in Table 5. Figures 14–16 show a comparison of attitude errors in the two different schemes. As is shown in the blue curves, attitude errors of the gyro-drift-corrected scheme diverge due to an inaccurate horizontal reference. So, the attitude accuracy becomes poor and the

Table 5. Simulation results of two different integration modes.

| Navigation error | Gyro-drift-corrected SINS /CNS scheme | | Proposed scheme | |
|--------------------------------|--|---------|-----------------|---------|
| | variance | maximum | variance | maximum |
| Easterly position error (m) | 203.54 | 343.20 | 63.79 | 206.81 |
| Northerly position error (m) | 78.49 | 147.33 | 42.21 | 114.07 |
| Total position error (m) | 84.09 | 343.22 | 42.90 | 208.75 |
| Easterly velocity error (m/s) | 0.169 | 0.298 | 0.039 | 0.147 |
| Northerly velocity error (m/s) | 0.125 | 0.323 | 0.045 | 0.123 |
| Total velocity error (m/s) | 0.086 | 0.363 | 0.032 | 0.168 |
| Pitch angle error (") | 4.05 | 7.47 | 0.94 | 2.66 |
| Yaw angle error (") | 5.12 | 9.34 | 0.96 | 3.26 |
| Roll angle error (") | 2.25 | 4.97 | 0.86 | 2.53 |
| Total angle error (") | 3.07 | 11.16 | 0.83 | 4.21 |

maximum error is more than $10''$. As the CNS can provide an accurate horizontal reference, attitude errors of the proposed SINS/CNS converge quickly and remain at about $5''$, as shown in the red curves. Therefore, through the aiding given by the CNS, the accuracy of SINS/CNS is significantly improved.

6. CONCLUSIONS. In this paper, a high-accuracy SINS/CNS integrated navigation scheme based on overall optimal correction is proposed to achieve long-endurance and accurate navigation. The following conclusions can be obtained through simulation and analysis:

- (1) Only one single large FOV star sensor needs to be installed on the body of a HALE UAV which will reduce the design cost. Without the need for temporal registration between two star sensors, the rapidity and accuracy of the system can be improved.
- (2) The traditional CNS positioning method depends on an orbital dynamics model, nonlinear filter and aid from SINS or a horizon sensor. However, the position determination algorithm proposed in this paper is based on just measurements of the star sensor and a refraction model. Therefore, the accuracy and reliability of system is enhanced, and calculation load is also reduced.
- (3) As CNS will provide attitude and position, the navigation errors of SINS can be continually revised. Compared with the gyro-drift-corrected SINS/CNS scheme, the navigation performance of the proposed SINS/CNS scheme is significantly improved.

Therefore, the proposed SINS/CNS scheme is suitable for a HALE UAV. It can also be applied to vehicles which are required to fly for a long time, such as near space vehicles, space shuttle vehicles and ballistic missiles.

ACKNOWLEDGEMENTS

This work was supported by the Natural Science Foundation of China (NSFC) (grant number 61233005, 61074157 and 61673040), the State Key Lab Foundation of Astronautical Dynamics of China (grant number 2012ADL-DW0201), the Joint Projects of NSFC-CNRS (grant number 61111130198), the Aeronautical Science Foundation of China (grant number 2015ZC51038 and

20160812004), and the Open Research Fund of State Key Laboratory of Space-Ground Information Technology (grant number 2015-SGII-KFJJ-DH-01). The authors would like to thank Mr Xuan Ming for his valuable suggestions.

REFERENCES

- Hays, P.B. and Roble, R.G (1967). Stellar spectra and atmospheric composition. *Journal of the Atmospheric Sciences*, **25**(6), 1101–1104.
- Høg, E., Fabricius, C., Makarov, V.V, Urban, S., Corbin, T., and Wycoff, G, et al. (2000). The tycho-2 catalogue of the 2.5 million brightest stars. *Astronomy & Astrophysics*, **355**(1), L27–L30.
- Hong, D., Liu, G, Chen, H. and Deng, C. (2010). Application of EKF for missile attitude estimation based on “SINS/CNS” integrated guidance system. *International Symposium on Systems and Control in Aeronautics and Astronautics, IEEE*, 1101–1104.
- He, Z., Wang, X. and Fang, J. (2014). An innovative high-precision SINS/CNS deep integrated navigation scheme for the Mars rover. *Aerospace Science and Technology*, **39**, 559–566.
- Li, H., Li, Y. and Ning, W. (2008). SINS/CNS/GNSS integrated navigation system based on CNS simulator for ballistic missile. *Journal of Projectiles Rockets Missiles & Guidance*, **28**(1), 61–63.
- Ma, P., Jiang, F. and Baoyin, H. (2015). Autonomous Navigation of Mars Probes by Combining Optical Data Viewing Martian Moons and SST Data. *The Journal of Navigation*, **68**(6), 1019–1040.
- Ning, X., Wang, L., Bai, X. and Fang, J. (2013). Autonomous satellite navigation using starlight refraction angle measurements. *Advances in Space Research*, **51**(9), 1761–1772.
- Qian, H., Sun, L., Cai, J. and Huang, W. (2014). A starlight refraction scheme with single star sensor used in autonomous satellite navigation system. *Acta Astronautica*, **96**, 45–52.
- Qu, C., Xu, H. and Tan, Y. (2011). SINS/CNS integrated navigation solution using adaptive unscented Kalman filtering. *International Journal of Computer Applications in Technology*, **41**(1–2), 109–116.
- Quan, W., Fang, J., Xu, F. and Sheng, W. (2008). Hybrid simulation system study of SINS/CNS integrated navigation. *IEEE Aerospace & Electronic Systems Magazine*, **23**(2), 17–24.
- Quan, W. and Fang, J. (2012). Research on FKF method based on an improved genetic algorithm for multi-sensor integrated navigation system. *The Journal of Navigation*, **65**(3), 495–511.
- Wang, X. and Ma, S. (2009). A celestial analytic positioning method by stellar horizon atmospheric refraction. *Chinese Journal of Aeronautics*, **22**(3), 293–300.
- Wang, X., Wang, B. and Li, H. (2012). An autonomous navigation scheme based on geomagnetic and starlight for small satellites. *Acta Astronautica*, **81**(1), 40–50.
- Wang, H., Zhou, W., Cheng, X. and Lin, H. (2012). Image smearing modeling and verification for strapdown star sensor. *Chinese Journal of Aeronautics*, **25**(1), 115–123.
- Wang, Y., Zheng, W., An, X., Sun, S. and Li, L. (2013). XNAV/CNS integrated navigation based on improved kinematic and static filter. *The Journal of Navigation*, **66**(6), 899–918.
- Wu, H., Yu, W. and Fang, J. (2006). Simulation of SINS/CNS integrated navigation system used on high altitude and long-flight-time unpiloted aircraft. *Acta Aeronautica Et Astronautica Sinica*, **27**(2), 299–304.
- Wu, X. and Wang, X. (2011). A SINS/CNS deep integrated navigation method based on mathematical horizon reference. *Aircraft Engineering and Aerospace Technology*, **83**(1), 26–34.
- Yang, J. and Wang, Y. (2013). Initial alignment error and navigation error compensation methods for SINS/CNS integration. *In Applied Mechanics and Materials*, **390**, 490–494.
- Yang, S., Yang, G, Zhu, Z. and Li, J. (2015). Stellar Refraction-Based SINS/CNS Integrated Navigation System for Aerospace Vehicles. *Journal of Aerospace Engineering*, **29**(2), 04015051.
- Yang, B., Si, F., Xu, F. and Zhou, W. (2014). Adaptive measurement model of navigation by stellar refraction based on multiple models switching. *Journal of Navigation*, **67**(4), 673–685.
- Zhang, T., and Zhang, J. (2009). An integrated inertial double-star/celestial navigation system for ballistic missile. *Computer Simulation*, **26**(3), 40–40.
- Zhang, D., Fu, K., Ge, S. and Tang, Z. (2014). Analysis of filtering methods for the SINS/CNS integrated navigation system of missile motion. *Intelligent Control and Automation, IEEE*, **103**, 3854–3859.